Structures of two bacterial resistance factors mediating tRNA-dependent aminoacylation of phosphatidylglycerol with lysine or alanine

Stefanie Hebecker[a,1], Joern Krausze[b,1], Tatjana Hasenkampf[a], Julia Schneider[a], Maike Groenewold[b], Joachim Reichelt[b], Dieter Jahn[a], Dirk W. Heinz[b], and Jürgen Moser[a,2]

[a]Institute of Microbiology, Technische Universität Braunschweig, 38106 Braunschweig, Germany; and [b]Department of Molecular Structural Biology, Helmholtz Centre for Infection Research, 38124 Braunschweig, Germany

Edited by Dieter Söll, Yale University, New Haven, CT, and approved July 16, 2015 (received for review June 9, 2015)

The cytoplasmic membrane is probably the most important physical barrier between microbes and the surrounding habitat. Aminoacylation of the polar head group of the phospholipid phosphatidylglycerol (PG) catalyzed by Ala-tRNA^{Ala}–dependent alanyl-phosphatidylglycerol synthase (A-PGS) or by Lys-tRNA^{Lys}–dependent lysyl-phosphatidylglycerol synthase (L-PGS) enables bacteria to cope with cationic peptides that are harmful to the integrity of the cell membrane. Accordingly, these synthases also have been designated as multiple peptide resistance factors (MprF). They consist of a separable C-terminal catalytic domain and an N-terminal transmembrane flippase domain. Here we present the X-ray crystallographic structure of the catalytic domain of A-PGS from the opportunistic human pathogen *Pseudomonas aeruginosa*. In parallel, the structure of the related lysyl-phosphatidylglycerol–specific L-PGS domain from *Bacillus licheniformis* in complex with the substrate analog L-lysine amide is presented. Both proteins reveal a continuous tunnel that allows the hydrophobic lipid substrate PG and the polar aminoacyl-tRNA substrate to access the catalytic site from opposite directions. Substrate recognition of A-PGS versus L-PGS was investigated using misacylated tRNA variants. The structural work presented here in combination with biochemical experiments using artificial tRNA or artificial lipid substrates reveals the tRNA acceptor stem, the aminoacyl moiety, and the polar head group of PG as the main determinants for substrate recognition. A mutagenesis approach yielded the complementary amino acid determinants of tRNA interaction. These results have broad implications for the design of L-PGS and A-PGS inhibitors that could render microbial pathogens more susceptible to antimicrobial compounds.

A-PGS | L-PGS | MprF | structure | tRNA

Bacteria can adapt rapidly to changing environmental conditions by controlling the physical properties of biological membranes (1). One important strategy is the tRNA-dependent aminoacylation of the polar head group of phosphatidylglycerol (PG) by aminoacyl-phosphatidylglycerol synthases (aa-PGSs). The resulting products alanyl-phosphatidylglycerol (A-PG) or lysyl-phosphatidylglycerol (L-PG) (Fig. 1) reduce the overall net negative charge of the membrane, making it less susceptible to cationic antimicrobial peptides (CAMPs). Such CAMPs often are synthesized as innate immunity host-defense peptides in response to bacterial infections (2–5). Fundamental work with the Gram-positive pathogen *Staphylococcus aureus* indicated aa-PGS–mediated nonsusceptibility to vancomycin (an antibiotic of last resort), resistance to host antimicrobial peptides (defensins), and protection against neutrophil killing (6–9). Accordingly, aa-PGS enzymes can be considered virulence factors and thus have been termed "multiple peptide resistance factors." In *Pseudomonas aeruginosa*, aminoacylation of PG also was found in response to acidic environmental conditions (2, 5), *inter alia*. *P. aeruginosa* is the dominant pathogen that colonizes the lung of patients suffering from cystic fibrosis. Because of the underlying defect in bicarbonate ion transport, acidification of the airway surface liquid contributes to cystic fibrosis pathogenesis (10). Furthermore, during inflammatory response local acidification by the production of acids was observed (11).

Aa-PGS catalysis is one of the rare instances in which a ribosomal aminoacyl-tRNA is used other than in protein biosynthesis. Aa-PGS enzymes are classified as (*i*) A-PGS, found, for example, in Gram-negative *P. aeruginosa*; (*ii*) L-PGS, found in Gram-positive *S. aureus*, *Bacillus anthracis*, and *Bacillus licheniformis*, *inter alia*; and (*iii*) aa-PGS enzymes with a broadened substrate specificity (synthesis mainly of L-PG together with A-PG) as described for *Bacillus subtilis* and *Enterococcus faecium* (2–5, 12). Recent results demonstrate that precise tuning of cellular A-PG and/or L-PG concentrations is fundamental for bacterial resistance (2). Furthermore, regulatory circuits including specific aminoacyl-phosphatidylglycerol (aa-PG) hydrolases have been described for *P. aeruginosa* and *E. faecium* (13, 14).

The aa-PGS enzymes consist of a separable, water-soluble C-terminal domain showing full enzymatic activity (4, 15). This domain contains all elements for the specific recognition of the ∼26 kDa water-soluble aminoacyl-tRNA (Ala-tRNA^{Ala} or Lys-tRNA^{Lys}) and for binding of the hydrophobic PG substrate (15). The N-terminal transmembrane domain anchors aa-PGS

Significance

Lipid homeostasis is a fundamental process for understanding antimicrobial susceptibility. Modification of the polar head group of phosphatidylglycerol into the respective aminoacyl-ester of phosphatidylglycerol is a widely used strategy to mediate bacterial resistance. Here we present the structures of the catalytic domains of aminoacyl-phosphatidylglycerol synthases from *Pseudomonas aeruginosa* and *Bacillus licheniformis*. These prototypical enzymes specifically catalyze the tRNA-dependent synthesis of alanyl-phosphatidylglycerol and lysyl-phosphatidylglycerol, respectively. A central tunnel architecture facilitates binding of the polar aminoacyl-tRNA molecule opposite the hydrophobic lipid substrate as a fundamental principle for the catalysis at the water–lipid interface. Specific inhibition of aminoacyl-phosphatidylglycerol synthases might be a promising strategy to render Gram-positive and Gram-negative pathogenic bacteria more susceptible to antimicrobial treatment.

Author contributions: S.H., J.K., and J.M. designed research; S.H., J.K., T.H., J.S., M.G., and J.R. performed research; S.H., J.K., J.R., D.J., D.W.H., and J.M. analyzed data; and S.H., J.K., D.J., D.W.H., and J.M. wrote the paper.

The authors declare no conflict of interest.

This article is a PNAS Direct Submission.

Data deposition: Crystallography, atomic coordinates, and structure factors reported in this paper have been deposited in the Protein Data Bank, www.pdb.org (accession nos. 4V34, 4V35, and 4V36).

[1]S.H. and J.K. contributed equally to this work.

[2]To whom correspondence should be addressed. Email: j.moser@tu-bs.de.

This article contains supporting information online at www.pnas.org/lookup/suppl/doi:10.1073/pnas.1511167112/-/DCSupplemental.

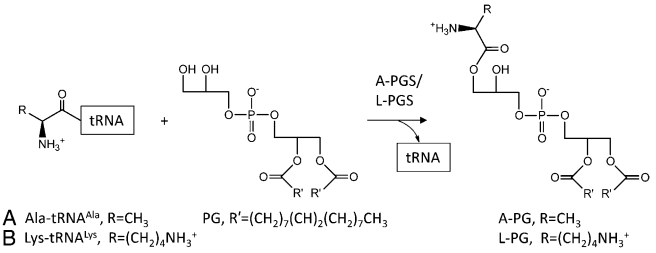

Fig. 1. tRNA-dependent aminoacylation of phosphatidylglycerol with alanine or lysine. A-PGS and L-PGS (also named "MprF") catalyzed the formation of A-PG (*A*) and L-PG (*B*), respectively.

proteins in the cytoplasmic membrane and harbors an additional translocase activity responsible for flipping the newly synthesized lipid into the outer leaflet of the cytoplasmic membrane (16).

This study presents the first, to our knowledge, structures of the catalytic A-PGS domain from *P. aeruginosa* together with the related L-PGS structure from *B. licheniformis* in the presence of a small substrate analog. Structural biology in combination with biochemical experiments using a series of artificial aminoacyl-tRNA or artificial lipid substrates allows the molecular understanding of aa-PGS substrate recognition as a basis for the future exploitation of this class of previously unidentified antimicrobial targets.

Results and Discussion

The determination of the crystal structures of the catalytic A-PGS and L-PGS domains from *P. aeruginosa* and *B. licheniformis* is summarized in Table S1 (effective resolution, 2.4 Å for each). The structural superposition of both structures with an rmsd of 1.1 Å is depicted in Fig. 2*A* (34.1% amino acid sequence identity; compare with alignment in Fig. S1). Despite this high degree of structural conservation, a marked specificity for the synthesis of A-PG or L-PG was observed for A-PGS and L-PGS in enzymatic assays using Ala-tRNA^{Ala} or Lys-tRNA^{Lys} as substrates, respectively (Fig. S2).

Both aa-PGS structures share a tandem repeated GNAT (GCN5-related N-acetyltransferase) fold (17). The topology diagram in Fig. 2*B* highlights GNAT domains 1 and 2 (colored light blue and blue, respectively) partially arranged with internal "pseudo-twofold symmetry" (rhombus), which share strands E and K (purple), respectively. Internal superposition of the central elements of GNAT domains 1 and 2 resulted in rmsds of 0.99 Å for A-PGS and 0.96 Å for L-PGS. Domain 2 shares the specific sequential arrangement of the GNAT fold (17, 18) with an insertion of two α-helices (8a and 9), whereas domain 1 lacks the most N-terminal β-strand of the superfamily.

The strongest structural homology (19) of both aa-PGS structures was found to the alanyl transferase FemX [Protein Data Bank (PDB) code 4II9], which is another Ala-tRNA^{Ala}–dependent enzyme involved in peptidoglycan interpeptide bridge formation. FemX catalyzes the transfer of L-Ala to the side chain of the ε-amino group of L-Lys of the peptidoglycan precursor UDP-MurNAc-pentapeptide (20). The core of the FemX protein also is composed of two GNAT domains that are related by pseudo-twofold symmetry (rmsd for internal superposition, 2.0 Å) (21). Structural domains 1 and 2 are separated by an extended cleft of 20 Å that is 15 Å deep to accommodate both the UDP-MurNAc-pentapeptide on GNAT domain 1 and the unpaired CCA acceptor arm of the charged tRNA on GNAT domain 2 (20). The superposition of GNAT domains 2 from A-PGS and FemX revealed an rmsd of 1.39 Å (GNAT domains 2 from L-PGS and FemX, 1.36 Å).

Notably, FemX was cocrystallized with a stable aminoacyl-tRNA analog. The peptidyl-RNA conjugate used mimics the peptide substrate in parallel with the instable Ala-tRNA^{Ala} cosubstrate, resulting in a structure that resolves the three terminal CCA nucleotides of the unpaired tRNA acceptor arm (20).

Structural superposition of the L-PGS (or A-PGS) structure with the FemX/peptidyl-RNA complex clearly localizes the terminal tRNA nucleotides in a defined cavity located on GNAT domain 2 of L-PGS (see Fig. 2*E*) (or A-PGS). This cavity is delineated mainly by secondary structure elements comprising a series of fully conserved amino acid residues [sequence excerpt; fully conserved residues are in bold, and residues in van der Waals distance are underscored: helix 6 and following loop region (**SDAWL**$_{713\ A\text{-}PGS}$/**SDEWL**$_{688\ L\text{-}PGS}$), strand I and following loop region (**DLMRV**HPD**APKLTM**$_{778\ A\text{-}PGS}$/**DLMRY**SKK**APKGIM**$_{742\ L\text{-}PGS}$), and helix 10 (**LRRFK**$_{840\ A\text{-}PGS}$/**FSGLRSFK**$_{814\ L\text{-}PGS}$)].

Notably, Phe839 and Lys840 of A-PGS (or Phe813 and Lys814 of L-PGS) are located in a spatial position identical to that of the catalytically relevant residues Phe304 and Lys305 of FemX. Therefore, the proposed CCA-binding mode was substantiated further by mutagenesis of related A-PGS residues. Mutational analyses revealed complete A-PGS inactivation with the mutagenesis of Lys840 and Phe839, as is consistent with related results for FemX mutagenesis (20). Therefore, we concluded that Lys840 and Phe839 have a central role in tRNA substrate interaction (compare Fig. S1 and Table S2).

In addition, residues Asp765 and Arg768 were identified as key catalytic A-PGS residues (yellow sticks in Fig. 2*C*). Remarkably, the L-PGS/FemX structural superposition depicted in Fig. 2*E* places the 3′ hydroxyl group of the terminal ribose moiety only 1.0 Å away from the cocrystallized L-lysine amide molecule (offset to the amide nitrogen of LYN, indicated by an asterisk in Fig. 2*E*). This compound (electron density depicted in Fig. S3) is a weak competitive inhibitor of L-PG synthesis (see Table S2). These structural and mutational analyses suggest a conserved binding mode for the unpaired CCA of the acceptor arm in aa-PGS and FemX proteins (compare Fig. 2*E*). The lower part of the L-lysine amide inhibitor-binding pocket is lined with a series of highly conserved amino acid residues, which are involved in an identical 3D network of polar interactions in the A-PGS and L-PGS structure (A-PGS/L-PGS: Ser709/Ser684, Glu720/Glu693, Tyr732/Tyr705, Asp765/Asp739, and Arg768/Arg742) (compare enlarged views in Fig. 2 *D* and *G*). Functional relevance for all these polar residues has been confirmed by mutagenesis as summarized in Table S2 (15). Combined interaction of Tyr732/Tyr705 and Asp765/Asp739 with the substrate α-amino group suggests an important role in the recognition of the substrate aminoacyl linkage. With regard to the catalyzed transesterification, residues Glu720/Glu693 and Ser709/Ser684 play a fundamental role in positioning Arg768/Arg742, which interacts directly with the α-carbonyl group of the cocrystallized inhibitor (compare Fig. 2 *D* and *G*). Structural and biochemical data suggest a nucleophilic attack of the 3′ hydroxyl group of PG on the Arg768/Arg742-activated α-carbonyl carbon of aminoacyl-tRNA.

Specific synthesis of A-PG or L-PG requires accurate recognition of Ala-tRNA^{Ala} versus Lys-tRNA^{Lys}. Inspection of the upper part of the aminoacyl-binding cavity of the L-PGS and A-PGS structure did not reveal any conserved or supplemental amino acid residues as direct determinants for the specific recognition (or steric exclusion) of the lysyl- versus the much smaller alanyl-substrate moiety. The four-aminobutyl side chain of the cocrystallized L-lysine amide is solely in contact with main-chain L-PGS atoms, which were found in an almost identical position in the related A-PGS structure (compare Fig. 2 *D* and *G*). One might argue that the sole amino acid moiety of the tRNA substrate does not account for the overall specificity of aa-PGS enzymes. Accordingly, we investigated whether the tRNA portion was a main aa-PGS determinant by using tRNA^{Lys} that was mischarged with the smaller amino acid alanine.

The highly specific A-PGS or L-PGS enzyme was analyzed in the presence of tRNA^{Lys} that was mischarged with the amino

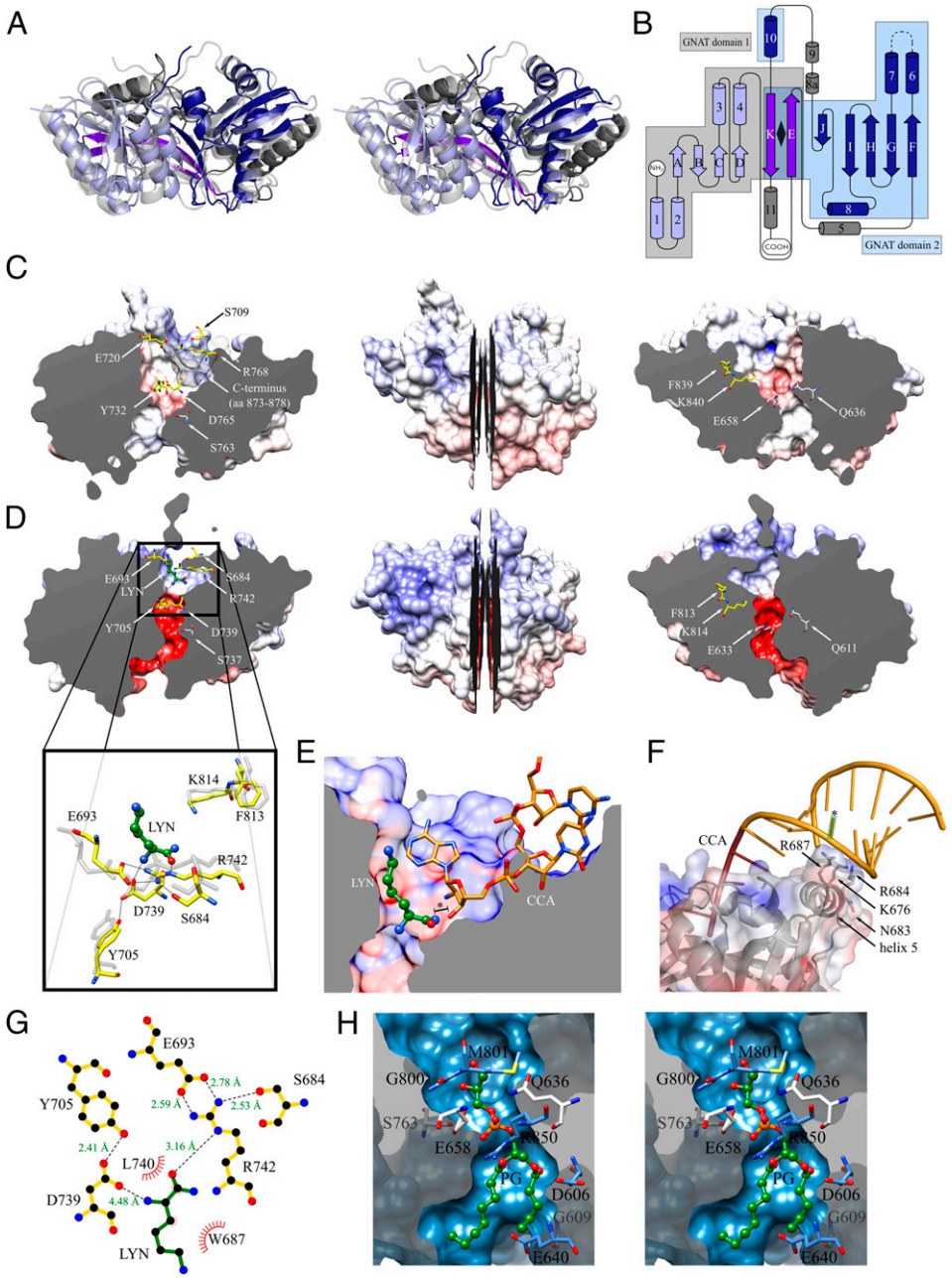

Fig. 2. X-ray structures of the catalytic domain of A-PGS from *P. aeruginosa* and L-PGS from *B. licheniformis*. (*A*) Structural superposition of A-PGS (light blue, blue, purple, and gray) and L-PGS (light gray) in a wall-eye stereo view. (*B*) Topology diagram of the tandem repeated GNAT fold of A-PGS and L-PGS. GNAT domains 1 and 2 (light blue and blue) share strands E and K (purple). The detailed sequence assignment for A-PGS and L-PGS is depicted in Fig. S1. (*C, Center*) A longitudinal section of the A-PGS structure from *P. aeruginosa*. (*Left* and *Right*) The resulting halves reveal a tunnel which contains the upper tRNA-binding pocket and the lower PG-binding tunnel. The key catalytic residues of A-PGS (yellow sticks) and residues located at the constriction of the tunnel (light gray sticks) and the C terminus (semitransparent gray surface) are located above the respective sectional plane. The protein is represented as a van der Waals surface and is colored according to its surface electrostatics [−20 (red) to +20 (blue) K_bT/e_c]. (*D*, *Center*) Longitudinal section of L-PGS in complex with the competitive inhibitor L-lysine amide. (*Left* and *Right*) The resulting halves reveal a tunnel that contains the L-lysine amide (LYN, green ball-and-stick representation)-binding site in the upper tRNA-binding pocket (*Left*) and the lower PG-binding cavity. Important amino acid residues are highlighted and colored as in *C*. The enlarged view in the left panel shows the polar interactions of key catalytic residues (yellow sticks) with the L-lysine amide, which is an analog of the aminoacyl moiety of the substrate Lys-$tRNA^{Lys}$. The position of the structurally related A-PGS amino acid residues is superimposed (light gray sticks). (*E*) Superposition of the FemX/tRNA structure (20) with the L-PGS/L-lysine amide complex reveals a plausible binding mode of the aminoacylated tRNA acceptor arm. A structural overlay of L-PGS/L-lysine amide with the FemX/tRNA complex localizes the terminal tRNA nucleotides (CCA) in a defined cavity of L-PGS. The 3′ hydroxyl oxygen atom of the terminal ribose is placed only 1.0 Å away from the cocrystallized L-lysine amide (LYN, offset indicated by asterisk). (*F*) Model for the interaction of A-PGS and tRNA. A representative tRNA molecule (PDB ID code 1TN1) was positioned onto the structure of A-PGS. The aminoacyl-binding pocket and the CCA-binding pocket were used as reference points. Mutational analysis for amino acid residues Lys676, Arg684, Arg687, and Asn683 located on helix 5 resulted in impaired A-PGS activity. The terminal base pairings G2-C71, G3-U70, and G4-C69 have been identified previously as tRNA-recognition elements (15). The theoretical position of the U70 base is indicated by an asterisk. (*G*) L-lysine amide (LYN) bound within the aminoacyl-binding pocket of L-PGS (yellow bonds). Hydrogen bonds as shown as dashed lines with distances indicated in Ångstroms. Generated with LIGPLOT (43). (*H*) Wall-eye stereo view of the lipid-binding tunnel of A-PGS. Enlarged view of the longitudinal section of Fig. 2*C*, *Right* indicating conserved amino acid residues (gray and blue). The functional role of amino acid residues Gln636, Glu658, and Ser763 (gray) was demonstrated by mutagenesis (see also Table S2). Docking calculations [using Autodock Vina (41)] revealed the theoretical binding mode of the PG lipid substrate (green sticks, representing PG C5:0/C8:0).

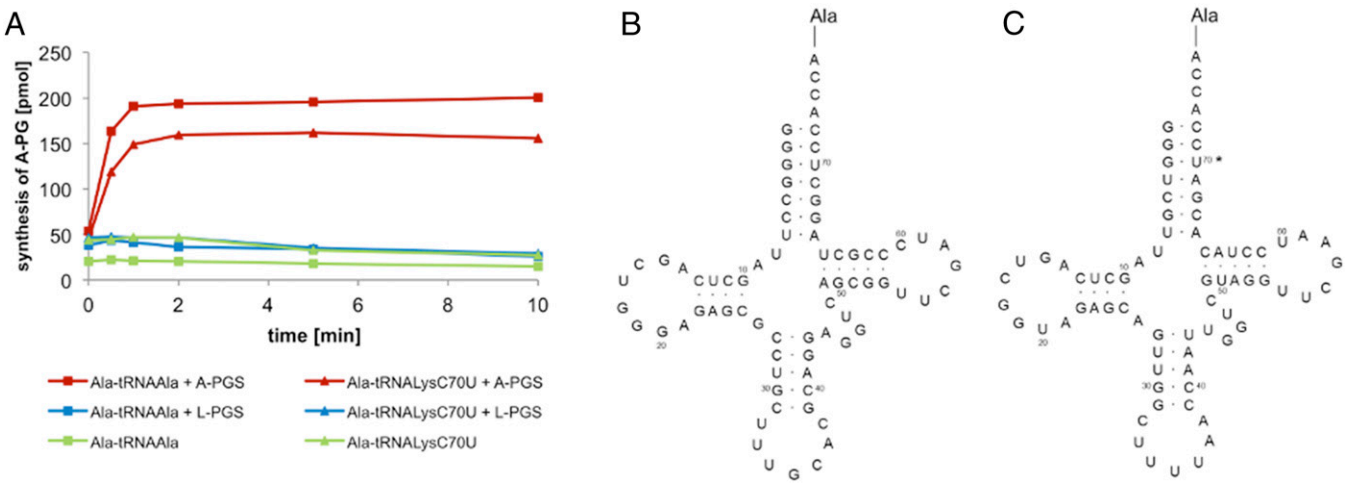

Fig. 3. A-PG synthesis of A-PGS and L-PGS using mischarged ^{14}C-Ala-tRNA^{Lys}C70U. (*A*) ^{14}C-Ala-tRNA^{Ala} or ^{14}C-Ala-tRNA^{Lys}C70U was used as substrate of A-PGS (0.2 μM) and L-PGS (1 μM) in combination with PG. Control reactions with purified L-PGS in the presence of the Lys-tRNA^{Lys} substrate revealed efficient L-PG formation (compare with Fig. S5). Synthesis of aa-PG was analyzed by lipid extraction and liquid scintillation analysis. (*B*) Sequence of Ala-tRNA^{Ala} from *B. licheniformis*. (*C*) Sequence of Ala-tRNA^{Lys}C70U from *P. aeruginosa*. The mutated base is indicated by an asterisk.

acid alanine (Ala-tRNA^{Lys}C70U; Fig. 3). The specific requirement for the C70U mutation within the synthesis of Ala-tRNA^{Lys}C70U is illustrated in the sequence comparison of the tRNA species we used, depicted in Fig. S4. This artificial Ala-tRNA^{Lys}C70U substrate was not accepted by L-PGS (compare Fig. 3 and Fig. S5). In contrast, the A-PGS enzyme revealed a relative activity of 80% compared with the natural Ala-tRNA^{Ala} substrate (Fig. 3). These experiments might indicate that the tRNA moiety in combination with the amino acid moiety of Ala-tRNA^{Ala} is relevant for A-PGS substrate recognition. These findings are supported further by earlier experiments (using artificial tRNA microhelices), which revealed the five terminal base pairings as important elements of A-PGS substrate recognition (15).

The theoretical comparison of the tRNA^{Ala} and the tRNA^{Lys} acceptor stem sequences shown in Fig. S4 reveals only base pairings G4–C69/U4–A69, C6–G67/G6–C67, and U70/C70 for the discrimination of tRNA^{Ala}/tRNA^{Lys}. However, the observed A-PGS activity in the presence of tRNA^{Lys}C70U indicates that G4, C69, C6, and G67 are nondiscriminating bases of A-PGS substrate recognition. Therefore, we concluded that U70 has a relevant role in A-PGS substrate recognition. In addition, specific substrate discrimination also might include dynamic interaction among aa-PGS and the overall tRNA substrate as exemplified for other transient protein/tRNA complexes (22, 23). Future cocrystallization experiments in the presence of sophisticated nonhydrolyzable aminoacyl-tRNA analogs might reveal such conformational rearrangements with relevance for the specific recognition of Ala-tRNA^{Ala} or Lys-tRNA^{Lys}.

Inspection of the protein surface of A-PGS and L-PGS revealed a series of conserved amino acid residues located on helix 5 (Lys676, Arg684, Arg687, and Asn683) as candidates for additional tRNA interaction. Mutagenesis of these residues into small polar residues always resulted in moderately retained activities (K676S, 29%; R684S, 21%; R687S, 13%; N683S, 71%; and N683D, 11%). In contrast, the individual charge reversal caused by glutamate insertion resulted in a complete loss of A-PGS activity, indicating a potential tRNA interaction. Subsequently, a representative tRNA structure from the Protein Data Bank (PDB ID code 1TN1) was positioned manually onto the structure of A-PGS and L-PGS using the aminoacyl-binding pocket and the CCA-binding pocket as points of reference. This experiment revealed the mutagenized amino acid residues of helix 5 (Lys676, Arg684, Arg687) in van der Waals distance from the previously determined recognition elements of the tRNA^{Ala} acceptor stem (base pairings G2–C71, G3–U70, and G4–C69). Fig. 2*F* shows an enlarged view of this A-PGS/tRNA acceptor stem interaction, and the overall models of tRNA/A-PGS and tRNA/L-PGS interaction are depicted in Fig. S6.

Aa-PGS catalysis requires the recruitment of the hydrophobic lipid substrate, whereas FemX binds the polar UDP-MurNAc-pentapeptide in an extended cleft located on GNAT domain 1 (20). Accordingly, we propose a completely unrelated aa-PGS substrate-binding mode with respect to PG. A comparison of the overall structure of aa-PGS and FemX reveals that the core secondary structural elements of GNAT domain 1 are tilted by up to 6 Å toward the domain interface, thereby closing the UDP-MurNAc-pentapeptide–binding cavity of FemX by virtue of helix 1 (PDGGLALT$_{577}$) and loop region ARRGRSMI$_{602}$ and also by an insertion (loop region EKGFSLGR$_{727}$) and the extension (LIAGGLTGL$_{878}$) located at the C terminus of A-PGS.

In Fig. 2 *C* and *D* an intersection of both aa-PGS proteins reveals a 23-Å tunnel with a diameter of 4–8 Å, which is connected directly to the aminoacyl-tRNA– binding cavity of A-PGS and L-PGS, respectively. This theoretical "backdoor entrance" is delineated by conserved residues of GNAT domains 1 and 2 (see Fig. S1) and provides an elegant solution for the aa-PGS catalysis at the water–lipid interface: The water-insoluble lipid substrate was placed into the lower part of the A-PGS tunnel by running a molecular docking simulation (Autodock Vina software in combination with PG C5:0/C8:0; PDB ligand ID code AGA). The relative positioning of the PG molecule used in the postulated lipid-binding site of A-PGS is depicted in Fig. 2*H*. The 3′ hydroxyl of the polar lipid head group protrudes toward the aminoacyl-binding site, whereas the branched diacylglycerol moiety appears to have a high degree of flexibility concerning the recognition of the respective fatty acid moieties of PG [C16:0/C19:0 *cis* 9, 10 cyclopropane predominant in *P. aeruginosa* (5, 24)]. This theoretical docking mode is in agreement with earlier experiments investigating A-PGS activity in the presence of artificial PG substrates (15). Modification of the respective fatty acid alkyl chains by (*i*) variation of saturation, (*ii*) fourfold methylation, (*iii*) using a monoacylated PG derivative, or (*iv*) using a short-chain C6 fatty acid PG variant did not hamper the activity of A-PGS. However, the alteration of the polar head group into an ethylene glycol moiety or by using diphosphatidylglycerol with a symmetrically branched glycerol moiety did not result in any detectable

A-PGS activity, indicating that the polar head group of PG is the dominant determinant of lipid substrate recognition (15).

The proposed PG substrate-binding mode was analyzed experimentally by site-directed mutagenesis of solvent-exposed amino acid residues located at the bottleneck that forms the connection to the aminoacyl-tRNA–binding site of A-PGS (see Fig. 2*C* and the close-up view depicted in Fig. 2*H*). Replacing residues Gln636, Glu658, and Ser763 (highlighted in light gray in Fig. 2*H*) with significantly bulkier side chains (tryptophane, arginine, or asparagine) resulted in only moderately retained activities of 6% for E658R, 13% for Q636R, 10% for Q636W, 23% for E658W, and 11% for S763N (Table S2). These biochemical and structural findings suggest the binding of the polar aminoacyl-tRNA molecule opposite the hydrophobic lipid substrate as a fundamental principle for the aa-PGS catalysis at the water–lipid interface. The elucidated modes of substrate recognition provide a framework for the future development of aa-PGS inhibitors as a new strategy to render pathogenic bacteria more susceptible to established antibiotics and also to the wide range of naturally occurring antimicrobial defense molecules of the human host.

Materials and Methods

Production and Purification of *P. aeruginosa* A-PGS and *B. licheniformis* L-PGS. Base pairs 1627–2643 of ORF PA0920 from *P. aeruginosa* PAO1 and base pairs 1555–2550 of ORF *yfiX* from *B. licheniformis* DSM13 were PCR-amplified using oligonucleotide pairs 1 and 2 and 3 and 4 (Table S3), respectively, and were cloned into the XmaI and SacI sites of pET52b(+) (Novagen) for expression with a cleavable N-terminal *Strep*-II-tag. The SerP (surface entropy reduction) server (25) was used to identify mutations that may facilitate optimized crystallization of A-PGS ($KGKE_{674}$ to $AGAA_{674}$). To exchange amino acid residues of the catalytic domain of A-PGS, the QuikChange kit (Agilent) was used according to the manufacturer's instructions in combination with oligonucleotide pairs 5 and 6 to 31 and 32.

A-PGS and L-PGS genes were expressed, and recombinant proteins were purified to apparent homogeneity as follows: Transformed *Escherichia coli* BL 21 (DE3) cells for the production of $A\text{-}PGS_{543–881}$ and Tuner (DE3) cells for production of $L\text{-}PGS_{519–850}$ were cultivated at 37 °C in LB medium supplemented with 100 μg/mL ampicillin. At an OD_{578} of 0.5, protein production was induced with 50 μM of isopropyl β-d-1-thiogalactopyranoside, and cells were shifted to 17 °C for 18 h. Selenomethionine-labeled surface mutant $A\text{-}PGS_{543–881}$ AGAA with 90% SeMet occupancy was produced as described elsewhere (26).

Cells were harvested by centrifugation and disrupted by a French press at 19,200 psi in lysis buffer [100 mM Tris·HCl (pH 7.5), 400 mM NaCl, 20 mM $MgCl_2$, 5% (wt/vol) glycerol, 2 mM DTT].

After ultracentrifugation for 1 h at 110,000 × *g* at 4 °C, the supernatant was applied to 1 mL of *Strep*-Tactin Superflow resin (IBA), which was equilibrated with lysis buffer. Following washing with 10 mL of lysis buffer and 10 mL of elution buffer 1 [20 mM Tris·HCl (pH 7.5), 200 mM NaCl, 0.5 mM $MgCl_2$, 5% (wt/vol) glycerol, 2 mM DTT] for $A\text{-}PGS_{543–881}$ AGAA and $A\text{-}PGS_{543–881}$, or alternatively elution buffer 2 [20 mM Tris·HCl (pH 7.5), 300 mM NaCl, 5 mM $MgCl_2$, 5% (wt/vol) glycerol, 2 mM DTT] for $L\text{-}PGS_{519–850}$, the proteins were liberated and eluted from the resin by cleavage of the *Strep*-II-tag via PreScission protease treatment (GE Healthcare). The GST-tagged protease was removed using Glutathione Sepharose 4FF (GE Healthcare). The elution fractions containing A-PGS and L-PGS proteins, respectively, were concentrated to ∼10 mg/mL using Vivaspin 15 centrifugal concentrators with a 10-kDa cutoff (Sartorius).

Protein Crystallization. Crystals were obtained in hanging-drop vapor-diffusion experiments at 4 °C by mixing 2 μL of protein with 2 μL of reservoir solution. Crystals of selenomethionine-labeled $A\text{-}PGS_{543–881}$ AGAA grew from a solution containing 7.5 mM $CoCl_2$, 85 mM Mes (pH 5.7), 1.53 M $(NH_4)_2SO_4$, and 15% (vol/vol) glycerol. Crystals of native $A\text{-}PGS_{543–881}$ AGAA grew from 85 mM Na-acetate (pH 6.37), 1.6 M $(NH_4)_2SO_4$, and 20% (vol/vol) glycerol. Crystals of $L\text{-}PGS_{519–850}$ were obtained from a solution of 0.2 M NaCl, 0.1 M phosphate-citrate (pH 4.2), and 10% (wt/vol) PEG3000 supplemented with 0.5 mM L-lysine amide. Needle-shaped crystals grew within 1–2 wk. Crystals were shock-cooled in liquid nitrogen. $L\text{-}PGS_{519–850}$ crystals were cryoprotected with 30% (vol/vol) glycerol in reservoir solution before cooling in liquid nitrogen.

Data Collection, Structure Determination, and Refinement. Diffraction data of A-PGS and L-PGS crystals were collected on beamline 14.2 (27) of the Berlin Electron Storage Ring Society for Synchrotron Radiation (BESSY) II electron storage ring (Berlin-Adlershof) and on beamline P11 (28) of the Positron-Electron Tandem Ring Accelerator (Petra) III at DESY (Hamburg, Germany). Integration and space group assignment were carried out with XDS (29). A crystal of selenomethionine-derivatized A-PGS was used for data collection at the absorption edge of selenium. The resulting anomalous signal was sufficient to obtain experimental phases in a single-wavelength anomalous dispersion experiment and to compute initial electron density with phenix.autosol (30). A first structural model was built by phenix.autobuild (30), which subsequently was improved by manual rebuilding in COOT (31) and refinement in phenix.refine (30). An improved A-PGS model was obtained through refinement against high-resolution data of a native A-PGS crystal. Diffraction data of L-PGS crystals showed significant anisotropy and were subjected to anisotropy correction using the anisotropy correction server (32). The phase problem was solved by molecular replacement with phaser (33) using a pruned A-PGS monomer as search model. Phaser placed two monomers in the asymmetric unit with reasonable confidence. However, the resulting electron density was poor. Hence, model and density were improved by alternate rebuilding and relaxation cycles with phenix.mr_rosetta (34) and then finalized through manual rebuilding and refinement. The complete data collection and refinement statistics are shown in Table S1.

A-PGS/L-PGS Enzyme Assay. The in vivo A-PGS and L-PGS activities were determined as described before (15). To validate the purified (mutant) proteins, our well-established in vitro activity assay was performed (15). In brief, an *E. coli* strain overproducing either alanyl-tRNA synthetase (15) or lysyl-tRNA synthetase (35) provided the substrate molecules PG and aminoacylated $tRNA^{Ala}$ or $tRNA^{Lys}$. The formation of A-PG or L-PG, respectively, was determined by liquid scintillation counting using radioactively labeled [1-^{14}C]-L-alanine (51 mCi/mmol; Moravek Biochemicals) or [U-^{14}C]-L-lysine (288 mCi/mmol; Moravek Biochemicals) (15).

Preparation, Purification, and Aminoacylation of RNA Transcripts. The $tRNA^{Ala}$ gene from *B. licheniformis,* the $tRNA^{Lys}$ gene from *P. aeruginosa*, and the sequence for $tRNA^{Lys}$C70U (carrying identity elements for misacylation with alanine by alanyl-tRNA synthetase; G3-C70 base pair mutated to G3-U70) were cloned into the pUC18 vector (using oligonucleotides 33–38). In vitro-transcribed tRNAs were purified via MonoQ chromatography, folded, and acylated with [1-^{14}C]-L-alanine (for $tRNA^{Ala}$) or [U-^{14}C]-L-lysine (for $tRNA^{Lys}$), as described elsewhere (15, 36).

Misacylation of $tRNA^{Lys}$ Using Alanyl-tRNA Synthetase. Substrate recognition of alanyl-tRNA synthetase is one of the rare instances in which only a single base pair of the acceptor stem acts as a major identity element of tRNA recognition (37). Therefore, native $tRNA^{Lys}$ from *P. aeruginosa* functions as a substrate of alanyl-tRNA synthetase because of the sole mutation of the base pairing G3-C70 into G3-U70 (36). Hence, in vitro synthesis of the misacylated Ala-$tRNA^{Lys}$C70U offers an alternative methodology to investigate aa-PGS substrate recognition. In vitro-transcribed $tRNA^{Lys}$C70U was misacylated efficiently in the presence of 0.42 μM of ^{14}C-Ala and 1 μM *E. coli* alanyl-tRNA synthetase (15). Synthesis of a related Lys-$tRNA^{Lys}$C70U is strongly hampered because a lysyl-tRNA synthetase revealed a loss of activity by a factor of >1,000 as the result of a G3-U70 mutation (36).

A-PGS/L-PGS Activity Assays in the Presence of Ala-$tRNA^{Ala}$ and Misacylated Ala-$tRNA^{Lys}$C70U. We used 0.42 μM of ^{14}C-Ala-$tRNA^{Ala}$ or ^{14}C-Ala-$tRNA^{Lys}$C70U as substrate for A-PGS (0.2 μM) and L-PGS (0.1, 1 μM, and 10 μM) in the presence of 2 mg/mL PG (Sigma-Aldrich) supplemented with 1.76 mg/mL Triton X-100 in the respective elution buffers. Synthesis of A-PG was analyzed by lipid extraction and liquid scintillation analysis. Control experiments using ^{14}C-Lys-$tRNA^{Lys}$ were performed to demonstrate L-PGS activity. This experimental setup was used to elucidate the overall contribution of the tRNA substrate moiety.

Structure-Based Sequence Analysis. Structure-based sequence analyses were calculated by the MatchMaker and MatchAlign subroutines of UCSF Chimera (38, 39). Figures were prepared with Pymol (40) and UCSF Chimera. Rmsds were calculated in Pymol.

Molecular Docking of PG. Docking calculations were performed by means of Autodock Vina (41) as part of the MGLTools package (mgltools.scripps.edu/) to investigate the binding mode of the lipid substrate. The PG ligand (PG C5:0/C8:0, PDB ligand ID AGA, from structure 1q16; ref. 42) was extracted from PDB, charges and rotational bonds were assigned, and no flexibility was allowed for side-chain residues for the A-PGS structure. The search

volume was assigned first to the whole A-PGS and then stepwise, limited to the lower part of the substrate tunnel to exclude docking to the outer shell of the molecule. All conformers showing diametrically opposed fatty acid moieties were considered biologically irrelevant. The theoretical lipid-binding mode depicted in Fig. 2*H* shows the best result, having the lowest binding energy of the remaining list.

ACKNOWLEDGMENTS. We thank the staffs of beamline P11 of Petra III and beamline 14.2 of BESSY II for their support. This work was supported by Deutsche Forschungsgemeinschaft Grants MO 1749/1-2 and HE 1852/14-2. Parts of this research were carried out at the light source Petra III at the German Electron Synchrotron, Hamburg, and at BESSY II, Berlin, both members of the Helmholtz Association.

1. Zhang YM, Rock CO (2008) Membrane lipid homeostasis in bacteria. *Nat Rev Microbiol* 6(3):222–233.
2. Arendt W, Hebecker S, Jäger S, Nimtz M, Moser J (2012) Resistance phenotypes mediated by aminoacyl-phosphatidylglycerol synthases. *J Bacteriol* 194(6):1401–1416.
3. Peschel A, et al. (2001) *Staphylococcus aureus* resistance to human defensins and evasion of neutrophil killing via the novel virulence factor MprF is based on modification of membrane lipids with l-lysine. *J Exp Med* 193(9):1067–1076.
4. Roy H, Ibba M (2009) Broad range amino acid specificity of RNA-dependent lipid remodeling by multiple peptide resistance factors. *J Biol Chem* 284(43):29677–29683.
5. Klein S, et al. (2009) Adaptation of *Pseudomonas aeruginosa* to various conditions includes tRNA-dependent formation of alanyl-phosphatidylglycerol. *Mol Microbiol* 71(3):551–565.
6. Pillai SK, et al. (2007) Daptomycin nonsusceptibility in *Staphylococcus aureus* with reduced vancomycin susceptibility is independent of alterations in MprF. *Antimicrob Agents Chemother* 51(6):2223–2225.
7. Pillai SK, et al. (2009) Development of reduced vancomycin susceptibility in methicillin-susceptible *Staphylococcus aureus*. *Clin Infect Dis* 49(8):1169–1174.
8. Peschel A (2002) How do bacteria resist human antimicrobial peptides? *Trends Microbiol* 10(4):179–186.
9. Kristian SA, Dürr M, Van Strijp JA, Neumeister B, Peschel A (2003) MprF-mediated lysinylation of phospholipids in *Staphylococcus aureus* leads to protection against oxygen-independent neutrophil killing. *Infect Immun* 71(1):546–549.
10. Coakley RD, et al. (2003) Abnormal surface liquid pH regulation by cultured cystic fibrosis bronchial epithelium. *Proc Natl Acad Sci USA* 100(26):16083–16088.
11. Simmen HP, Battaglia H, Giovanoli P, Blaser J (1994) Analysis of pH, pO_2 and pCO_2 in drainage fluid allows for rapid detection of infectious complications during the follow-up period after abdominal surgery. *Infection* 22(6):386–389.
12. Samant S, Hsu FF, Neyfakh AA, Lee H (2009) The *Bacillus anthracis* protein MprF is required for synthesis of lysylphosphatidylglycerols and for resistance to cationic antimicrobial peptides. *J Bacteriol* 191(4):1311–1319.
13. Arendt W, Groenewold MK, Hebecker S, Dickschat JS, Moser J (2013) Identification and characterization of a periplasmic aminoacyl-phosphatidylglycerol hydrolase responsible for *Pseudomonas aeruginosa* lipid homeostasis. *J Biol Chem* 288(34): 24717–24730.
14. Smith AM, Harrison JS, Sprague KM, Roy H (2013) A conserved hydrolase responsible for the cleavage of aminoacylphosphatidylglycerol in the membrane of *Enterococcus faecium*. *J Biol Chem* 288(31):22768–22776.
15. Hebecker S, et al. (2011) Alanyl-phosphatidylglycerol synthase: Mechanism of substrate recognition during tRNA-dependent lipid modification in *Pseudomonas aeruginosa*. *Mol Microbiol* 80(4):935–950.
16. Ernst CM, et al. (2009) The bacterial defensin resistance protein MprF consists of separable domains for lipid lysinylation and antimicrobial peptide repulsion. *PLoS Pathog* 5(11):e1000660.
17. Dyda F, Klein DC, Hickman AB (2000) GCN5-related N-acetyltransferases: A structural overview. *Annu Rev Biophys Biomol Struct* 29:81–103.
18. Vetting MW, et al. (2005) Structure and functions of the GNAT superfamily of acetyltransferases. *Arch Biochem Biophys* 433(1):212–226.
19. Holm L, Rosenstrom P (2010) Dali server: Conservation mapping in 3D. *Nucleic Acids Res* 38(Web Server issue):W545–549.
20. Fonvielle M, et al. (2013) The structure of FemX(Wv) in complex with a peptidyl-RNA conjugate: Mechanism of aminoacyl transfer from Ala-tRNA(Ala) to peptidoglycan precursors. *Angew Chem Int Ed Engl* 52(28):7278–7281.
21. Biarrotte-Sorin S, et al. (2004) Crystal structures of *Weissella viridescens* FemX and its complex with UDP-MurNAc-pentapeptide: Insights into FemABX family substrates recognition. *Structure* 12(2):257–267.
22. Francklyn C, Perona JJ, Puetz J, Hou YM (2002) Aminoacyl-tRNA synthetases: Versatile players in the changing theater of translation. *RNA* 8(11):1363–1372.
23. Francklyn CS (2008) DNA polymerases and aminoacyl-tRNA synthetases: Shared mechanisms for ensuring the fidelity of gene expression. *Biochemistry* 47(45): 11695–11703.
24. Hancock IC, Meadow PM (1969) The extractable lipids of *Pseudomonas aeruginosa*. *Biochim Biophys Acta* 187(3):366–379.
25. Goldschmidt L, Cooper DR, Derewenda ZS, Eisenberg D (2007) Toward rational protein crystallization: A Web server for the design of crystallizable protein variants. *Protein Sci* 16(8):1569–1576.
26. Li Z, Nimtz M, Rinas U (2011) Optimized procedure to generate heavy isotope and selenomethionine-labeled proteins for structure determination using *Escherichia coli*-based expression systems. *Appl Microbiol Biotechnol* 92(4):823–833.
27. Mueller U, et al. (2012) Facilities for macromolecular crystallography at the Helmholtz-Zentrum Berlin. *J Synchrotron Radiat* 19(Pt 3):442–449.
28. Meents A, et al. (2013) Development of an in-vacuum x-ray microscope with cryogenic sample cooling for beamline P11 at PETRA III. *Proc SPIE* 8851:88510K (abstr).
29. Kabsch W (2010) Xds. *Acta Crystallogr D Biol Crystallogr* 66(Pt 2):125–132.
30. Adams PD, et al. (2010) PHENIX: A comprehensive Python-based system for macromolecular structure solution. *Acta Crystallogr D Biol Crystallogr* 66(Pt 2):213–221.
31. Emsley P, Lohkamp B, Scott WG, Cowtan K (2010) Features and development of Coot. *Acta Crystallogr D Biol Crystallogr* 66(Pt 4):486–501.
32. Strong M, et al. (2006) Toward the structural genomics of complexes: Crystal structure of a PE/PPE protein complex from *Mycobacterium tuberculosis*. *Proc Natl Acad Sci USA* 103(21):8060–8065.
33. McCoy AJ, et al. (2007) Phaser crystallographic software. *J Appl Cryst* 40(Pt 4):658–674.
34. Terwilliger TC, et al. (2012) phenix.mr_rosetta: Molecular replacement and model rebuilding with Phenix and Rosetta. *J Struct Funct Genomics* 13(2):81–90.
35. Ibba M, Bono JL, Rosa PA, Söll D (1997) Archaeal-type lysyl-tRNA synthetase in the Lyme disease spirochete *Borrelia burgdorferi*. *Proc Natl Acad Sci USA* 94(26):14383–14388.
36. Ambrogelly A, Frugier M, Ibba M, Söll D, Giegé R (2005) Transfer RNA recognition by class I lysyl-tRNA synthetase from the Lyme disease pathogen *Borrelia burgdorferi*. *FEBS Lett* 579(12):2629–2634.
37. Hou YM, Schimmel P (1988) A simple structural feature is a major determinant of the identity of a transfer RNA. *Nature* 333(6169):140–145.
38. Pettersen EF, et al. (2004) UCSF Chimera–a visualization system for exploratory research and analysis. *J Comput Chem* 25(13):1605–1612.
39. Yang Z, et al. (2012) UCSF Chimera, MODELLER, and IMP: An integrated modeling system. *J Struct Biol* 179(3):269–278.
40. Schrödinger L (2010) The PyMOL molecular graphics system (Schrödinger, LLC, New York), Version 1.5.0.4.
41. Trott O, Olson AJ (2010) AutoDock Vina: Improving the speed and accuracy of docking with a new scoring function, efficient optimization, and multithreading. *J Comput Chem* 31(2):455–461.
42. Bertero MG, et al. (2003) Insights into the respiratory electron transfer pathway from the structure of nitrate reductase A. *Nat Struct Biol* 10(9):681–687.
43. Wallace AC, Laskowski RA, Thornton JM (1995) LIGPLOT: A program to generate schematic diagrams of protein-ligand interactions. *Protein Eng* 8(2):127–134.
44. Sievers F, et al. (2011) Fast, scalable generation of high-quality protein multiple sequence alignments using Clustal Omega. *Mol Syst Biol* 7:539.
45. Afonine PV, Headd JJ, Terwilliger TC, Adams PD (2013) New tool: Phenix.real_space_refine. *Computational Crystallography Newsletter* 4:51–58.
46. Francklyn C, Schimmel P (1989) Aminoacylation of RNA minihelices with alanine. *Nature* 337(6206):478–481.
47. Tamura K, Himeno H, Asahara H, Hasegawa T, Shimizu M (1992) In vitro study of *E. coli* tRNA(Arg) and tRNA(Lys) identity elements. *Nucleic Acids Res* 20(9):2335–2339.
48. Karplus PA, Diederichs K (2012) Linking crystallographic model and data quality. *Science* 336(6084):1030–1033.